ADVANCED FUNCTIONAL MATERIALS
www.afm-journal.de

www.MaterialsViews.com

The Role of Point Defects in the Mechanical Behavior of Doped Ceria Probed by Nanoindentation

Roman Korobko, Seong K. Kim, Sangtae Kim, Sidney R. Cohen, Ellen Wachtel, and Igor Lubomirsky**

The influence of dopant size and oxygen vacancy concentration on the room temperature elastic modulus and creep rate of ceria doped with Pr^{4+}, Pr^{3+}, Lu^{3+}, and Gd^{3+}, is investigated using a nanoindentation technique. Measurements are conducted with both fast (15 mN s^{-1}) and slow (0.15 mN s^{-1}) loading modes, including a load-hold stage at 150 mN of 8 s and 30 s, respectively. Based on the data obtained using the fast loading mode, it is found that: 1) the dopant size is a primary determinant of the elastic modulus—the larger dopants (Pr^{3+} and Gd^{3+}) produce lower unrelaxed moduli which are independent of the oxygen vacancy concentration. 2) The rearrangement of point defects is the major source of room temperature creep observed during load-hold. Pr^{3+}- and Gd^{3+}-doped ceria display the higher creep rates: due to their large size, they repel oxygen vacancies (V_O), thereby promoting the formation of O_I–Ce_{Ce}–V_O complexes that are capable of low temperature rearrangement. Lower creep rates are observed for Pr^{4+}- and Lu^{3+}-doped ceria: the former has no vacancies and the latter, immobile vacancies. 3) Nanoindentation is a practical technique for identifying materials with labile point defects, which may indicate useful functionality such as high ionic conductivity, large electrostriction, and inelasticity.

1. Introduction

Elastic properties of Gd-doped ceria, one of the most extensively studied oxygen ion conductors,[1–3] deviate strongly from linear behavior below 250 °C,[4–6] and, as was recently reported, exhibit giant electrostriction at room temperature.[7] Growing interest in miniature fuel cells operating at moderate temperatures,[2,8–11] as well as the potential application of the giant electrostriction effect for actuators, poses a number of questions with respect to the possible roles of the oxygen vacancies and dopants, both isovalent and aliovalent, on the mechanical properties. The dependence of the elastic modulus on the concentration of dopants in ceria remains a matter of both theoretical and experimental debate.[12–19]

Nanoindentation has developed into an established technique for investigating both quasi-static and dynamic elastic modulus, as well as hardness, at nanoscale volumes and depths. The technique involves pressing a hard and stiff indenter tip of calibrated shape into a surface with force and displacement control in the nano-Newton and nanometer range, respectively. Under certain limiting assumptions,[20,21] hardness and modulus are obtained directly from the load versus displacement curves. Furthermore, creep behavior can be investigated by monitoring displacement relaxation during a period of fixed load. Nanoindentation measurements[22,23] showed that the unrelaxed elastic modulus of bulk $Ce_{1-x}Gd_xO_{2-x/2}$ (x =0–0.2) ceramics is independent of Gd content, when observed on a time scale of ≈20 s. It was also shown that $Ce_{1-x}Gd_xO_{2-x/2}$ ceramics exhibit primary (initial) creep during the load–hold stage of the measurements due to the time-dependent diffusion and motion of atoms and/or movement of dislocations in the stress field. Creep at room temperature is rather unusual in a ceramic material with a melting point above 2600 K and with cations in a high oxidation state, which makes the creep in ceria particularly interesting. Characteristic of primary creep, the displacement, Δu, is given by $\Delta u = A\sqrt[3]{t}$, where t is the time which has elapsed from the beginning of the load–hold phase; and A is the creep rate constant. A reaches a maximum at ≈3 mol% Gd and decreases linearly in the range 5–20 mol%. In these measurements, creep cannot be attributed to grain boundaries and/or movement of dislocations. The indentation depth (<900 nm), as described in previous work,[22] was smaller than the grain size (>1.5 μm) and movement of dislocations in ceramics at low temperatures is highly unlikely. We have attributed the presence of creep to the large concentration of point defects in $Ce_{1-x}Gd_xO_{2-x/2}$, the structural consequences of which have been extensively studied by extended X-ray absorption fine structure spectroscopy

R. Korobko, Dr. E. Wachtel, Prof. I. Lubomirsky
Department of Materials and Interfaces
Weizmann Institute of Science
Rehovot 76100, Israel
E-mail: Igor.Lubomirsky@weizmann.ac.il
S. K. Kim, Prof. S. Kim
Department of Chemical Engineering and Materials Science
University of California
Davis, CA 95616, USA
E-mail: chmkim@ucdavis.edu
Dr. S. R. Cohen
Chemical Research Support Unit
Weizmann Institute of Science
Rehovot 76100, Israel

DOI: 10.1002/adfm.201301536

© 2013 WILEY-VCH Verlag GmbH & Co. KGaA, Weinheim

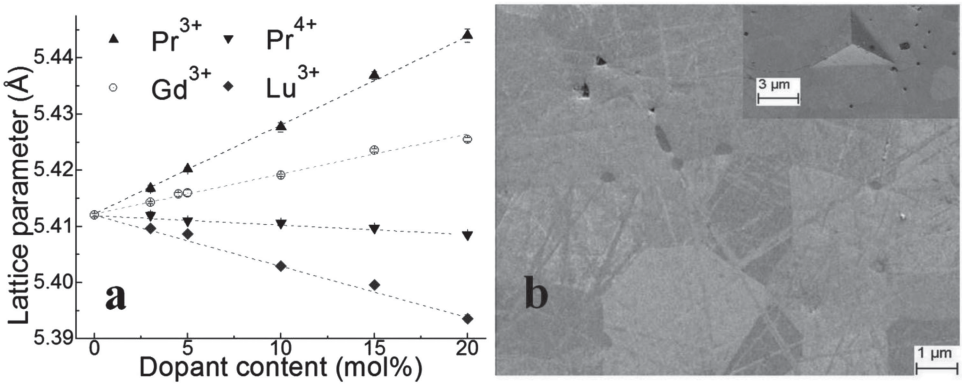

Figure 1. a) Fluorite unit cell parameter of $Ce_{1-x}Lu_xO_{2-x/2}$, $Ce_{1-x}Pr_xO_{2-x/2}$, $Ce_{1-x}Gd_xO_{2-x/2}$, and $Ce_{1-x}Pr_xO_2$ (x =0.0–0.2) ceramics used for this study. The data for Gd-doped ceria can be found in the literature.[22] b) SEM image of the cross section of $Ce_{0.9}Lu_{0.1}O_{1.95}$ illustrating typical grain size and structure. The crisscross lines are polishing marks. Less than one percent of the image area is occupied by pores, which implies that their contribution to the total volume is negligible. Inset: SEM image of a typical indenter mark.

(EXAFS),[24–26] synchrotron X-ray diffraction,[27] and neutron diffraction.[28,29] It was shown that the origin of both the inelastic behavior and the giant electrostriction may be related to the rearrangement of O_I–Ce_{Ce}–V_O (V_O are oxygen vacancies) complexes, which are labile in response to applied stress.[7,25,26] The fluorite lattice is viewed as distorting locally, in particular along the Ce_{Ce}–V_O direction, in a mode similar to that found for the double fluorite phase of Gd-rich ceria.[30] At room temperature, X-ray diffraction (XRD) peaks characteristic of double fluorite symmetry appear already at 25 mol% Gd.[27,31,32]

In the present study, we have extended the nanoindentation measurements to $Ce_{1-x}M_xO_{2-\delta}$, $M = Pr^{3+}$, Pr^{4+}, Lu^{3+}, where $x = 0$–0.2 and $\delta = 0$ (Pr^{4+}) or $x/2$ (Pr^{3+} or Lu^{3+}). These measurements allow the comparison of materials with a large concentration of oxygen vacancies that are mobile at high temperatures, ($M = Pr^{3+}$, Gd^{3+}) with materials without vacancies ($M = Pr^{4+}$) and materials with a large concentration of immobile vacancies ($M = Lu^{3+}$). The choice of dopants was guided by the ionic radii. The crystal radius of Pr^{3+} (126.6 pm) is much larger that of the host Ce^{4+} (111 pm), whereas Pr^{4+} and Lu^{3+}, despite the difference in their charge, have crystal radii close to that of Ce^{4+}: 110 pm and 117.7 pm, respectively.[33] Our data demonstrate 1) that the dopant radius, rather than the oxygen vacancy concentration, is a primary determinant of the elastic modulus; 2) that the rearrangement of point defects is the major cause of creep at room temperature; and 3) that nanoindentation is a practical technique for identifying materials with labile point defects,[26] which may potentially indicate practical functionality such as high ionic conductivity,[1,34,35] large electrostriction,[7] and inelasticity.[36]

2. Results and Discussion

The XRD patterns of $Ce_{1-x}Lu_xO_{2-x/2}$, $Ce_{1-x}Pr_xO_{2-x/2}$, $Ce_{1-x}Gd_xO_{2-x/2}$, and $Ce_{1-x}Pr_xO_2$ (x = 0.0-0.2) could be indexed according to fluorite symmetry (*Fm*–3*m*) (see Supporting Information). The data for Gd-doped ceria can be found elsewhere.[22] The as-prepared samples doped with Pr^{3+} display a linear increase of lattice parameter with Pr^{3+}-content (**Figure 1** a).[37,38] We must therefore conclude that, although all samples were sintered for 5 h in air at 1400 °C with heating/cooling rates of 5 °C min^{-1} (see the Experimental Section), this treatment was not sufficient for the oxidation of Pr to take place. The large majority of Pr remained in oxidation state +3. Annealing of the Pr-doped sample in air at 400, 450, and 370 °C for 12 h, and subsequent cooling at 5 °C min^{-1}, does not cause complete oxidation. However, after annealing in oxygen for at least 12 h at 380 °C, the lattice parameter of the Pr-doped ceramics displayed a small decrease with Pr-concentration (Figure 1a). This is evidence for the oxidation of Pr to the +4 state, in agreement with previous XRD studies of chemical expansion/contraction by Tuller and coauthors,[37,38] and XAFS data from previous work.[39]

According to scanning electron microscopy (SEM) images (Figure 1b), the grain size of all ceramics was ≈3 µm with pores occupying <1% of the image area. The latter observation corroborates the results of the Archimedes technique, showing that sample densities are ≥95% of theoretical density. Porosity reduces the actual amount of material stressed by the indentor; but in our case, the average porosity is so low that resulting variations in the measured mechanical response should not be larger than the inherent measurement uncertainty. The nanoindentation measurements (**Figure 2**) were performed with both "slow" 0.15 mN s^{-1} and "fast" 15 mN s^{-1} load application until a maximum load of 150 mN, followed by an 8 s (fast) or 30 s (slow) hold stage and then load release at the same rates (see the Experimental Section). The differences between the elastic modulus measured in the "slow" and "fast" modes are considerable, with the latter providing far more statistically significant results. For the case of the Pr^{3+} dopant, the average elastic modulus obtained in the fast mode is 219 ± 11 GPa approximately independent of Pr content for x = 0–0.2 (**Figure 3**). These results are very similar to those obtained for $Ce_{1-x}Gd_xO_{2-x/2}$ (216 ± 12 GPa)[22] for x = 0–0.2. Introducing Pr^{4+} and Lu^{3+} into pure ceria increases the elastic modulus, which reaches a maximum at 5 mol% and 3 mol% for Pr^{4+} and Lu^{3+} respectively. The elastic modulus becomes approximately

© 2013 WILEY-VCH Verlag GmbH & Co. KGaA, Weinheim

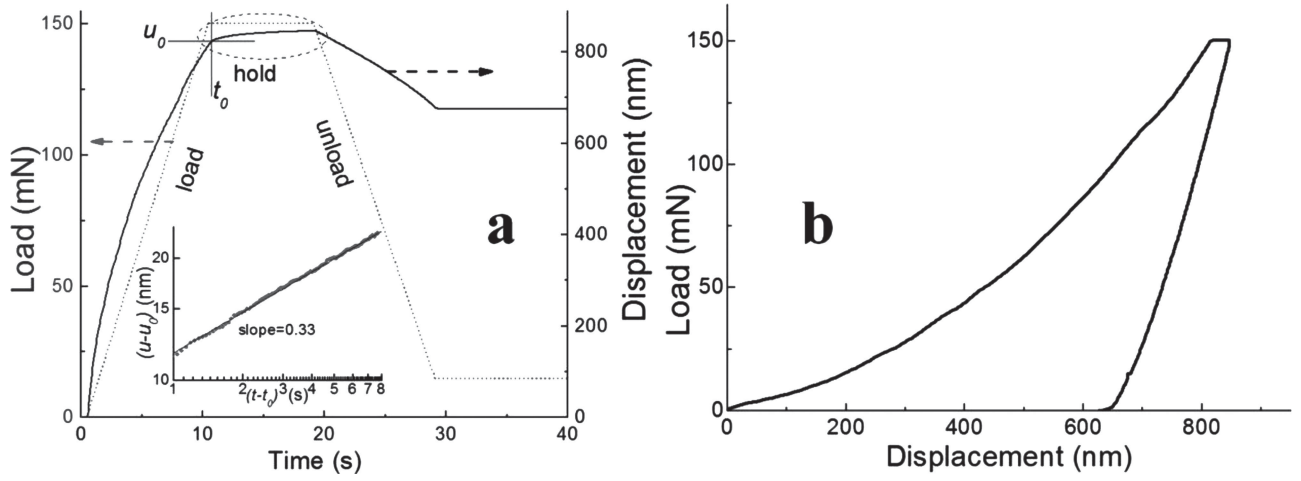

Figure 2. a) Representative displacement–time and load–time dependence for "fast" nanoindentation loading of a ceria pellet with 15 mol% Pr^{4+}. Inset: log–log plot of displacement vs time during the hold phase, indicating that the displacement is proportional to $\sqrt[3]{t}$. b) Typical load–displacement (depth) curve.

independent of dopant concentration, with average value within the range of 10–20 mol%: 247 ± 12 GPa and 254 ± 10 GPa for Pr^{4+} and Lu^{3+}, respectively (Figure 3). The nano-hardness (ratio of maximum load to contact area) values for all samples are consistently higher for the fast-mode measurements (Figure 3). However, nano-hardness for the Pr^{3+} dopant ($Ce_{1-x}Pr_xO_{2-x/2}$) increases monotonically with increasing dopant concentration, whereas the nano-hardness for Pr^{4+} and Lu^{3+} dopants displays a weak, irregular dependence on dopant concentration within the range $x = 0.05$–0.2.

All ceramics exhibited primary creep under constant load of 150 mN. During the creep process, the time dependence of the displacement was determined to be: $(u - u_0) = A\sqrt[3]{(t - t_0)}$ (Figure 2a inset), where $(u–u_o)$ is the displacement and $(t–t_o)$ is the time elapsed from the onset of load–hold. The magnitude of the creep rate constant, A, depends strongly on the nature of the dopant. For the case of Pr^{3+} (and Gd^{3+})[22] the creep rate reaches a maximum at 3 mol% and decreases linearly with dopant concentration between 10–20 mol% (**Figure 4**). One should note that in this range the creep rate of Pr^{3+} and Gd^{3+} doped ceria are similar. Even small amounts of Pr^{4+} or Lu^{3+} in ceria suppress creep. For 5–20 mol% Pr^{4+} (Figure 4), the creep rate is essentially independent of the dopant concentration and is 30–40% lower than that of pure ceria. Remarkably, despite the fact that the Lu^{3+} doped ceria samples contain the same concentration of vacancies as Pr^{3+}- and Gd^{3+}-doped ceria samples, the creep rate in the presence of Lu^{3+} is the lowest of the three. Suppression of creep is constant between 3–10 mol% Lu^{3+}, after which the creep decreases with a slope similar to that of the Pr^{3+}- or Gd^{3+}-doped samples.

Comparing the mechanical properties of Pr^{3+}-, Pr^{4+}-, and Lu^{3+}-doped ceria with those of Gd^{3+}-doped ceria,[22] we identify two trends. Pr^{3+}- and Gd^{3+}-doped ceramics display similar values for the elastic modulus and similar creep behavior despite the fact that the crystal radii of Pr^{3+} and Gd^{3+} are quite different, 126.6 pm and 119.3 pm, respectively. However, both radii are considerably larger than that of the host Ce^{4+} (111 pm). Notably, both materials are good oxygen ion conductors at elevated temperatures.[1,34] On the other hand, the ionic radii of Pr^{3+} and Lu^{3+} are very close to that of the host Ce^{4+}. Doping with these ions causes an increase in both the elastic modulus and nano-hardness values and a decrease in the creep rate, all with respect to the parameters of pure ceria. In light of the fact that the high temperature mobility of vacancies in doped ceria decreases with decreasing ionic radius of the dopant,[1,37] it is perhaps not surprising that the elastic properties of Pr^{4+}- and Lu^{3+}-doped ceria are similar to one another. Pr^{4+}-doped ceria has almost no oxygen vacancies, whereas Lu^{3+}-doped ceramics contain as many vacancies as Pr^{3+}- and Gd^{3+}-doped ceria, but with low mobility. It is clear that vacancy concentration alone cannot govern the dependence of the elastic modulus on doping up to 20 mol%. Instead, the radius of the dopant appears to be an important determining factor.

Analysis of the creep data provides additional insight into the role of the point defects and the nature of their interactions. As noted above, grain boundaries in doped ceria do not contribute to the room temperature creep measured by the nanoindentation technique. The ≈10 GPa applied stress (150 mN on a 3 μm diameter grain) is ≈10% of the shear modulus (less than 5% of the elastic modulus), and the maximum indentation depth is less than half the average grain size. Under these conditions, material transfer by diffusion at a grain boundary cannot produce the ≈10 nm displacement observed within 8 s.[38] We note that in doped ceria, cation diffusion only becomes measureable above 1000 K with typical creep time on the order of hours for strain of a few tenths of a percent.[40–42] This leaves only dislocation movement and rearrangement of the labile O_7–Ce_{Ce}–V_O complexes as possible sources of creep. However, dislocation movement, if it occurs, should be strongly impeded by dislocation pinning on the part of the dopants; the larger the difference between the crystal radius of the dopant and that of the host, the lower the creep.[43,44] The fact that 3 mol% of the large dopants, Pr^{3+} and Gd^{3+}, produces an increase in the creep rate while the same doping level with Pr^{4+} and Lu^{3+} suppresses creep, in

© 2013 WILEY-VCH Verlag GmbH & Co. KGaA, Weinheim

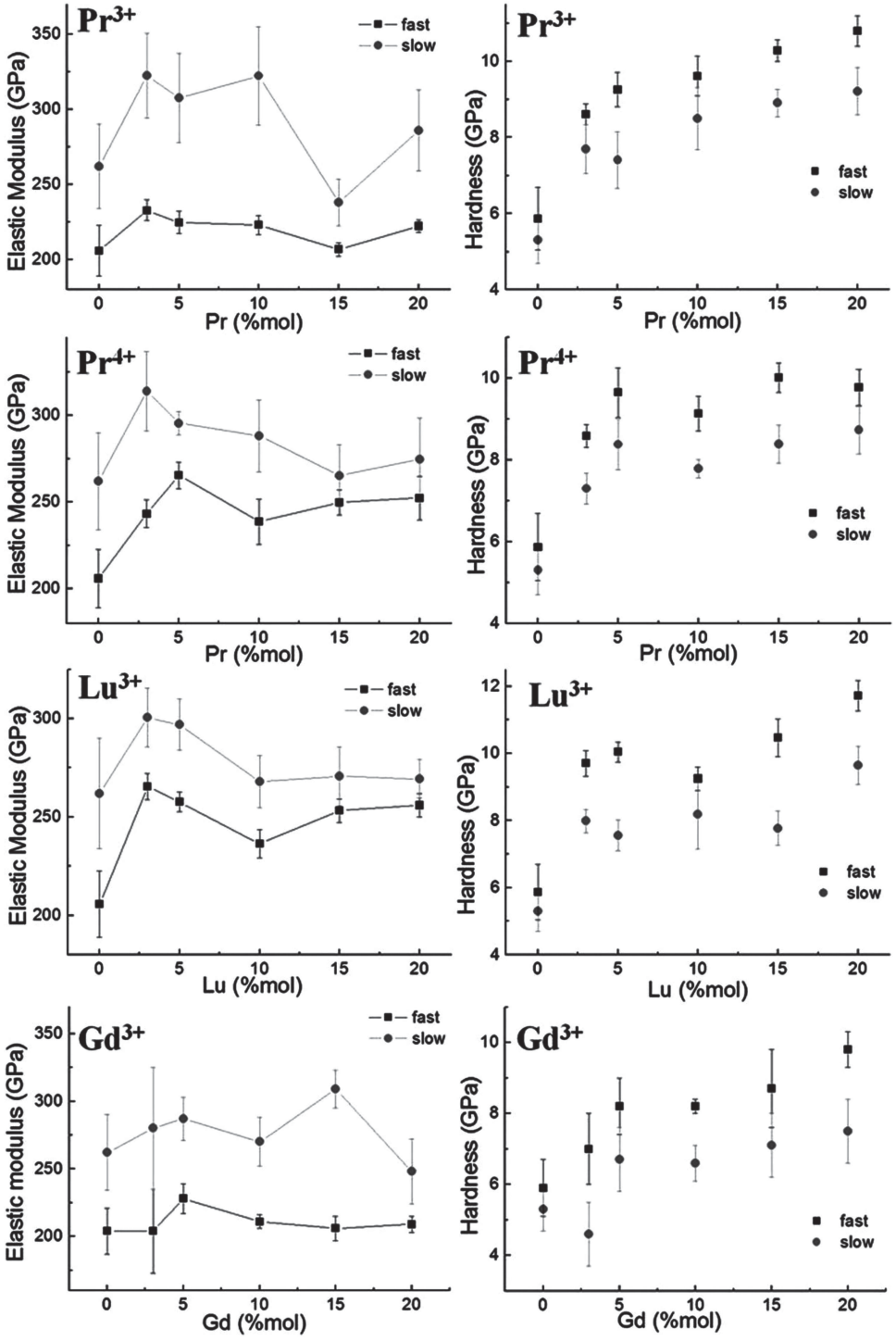

Figure 3. Elastic modulus and nano-hardness derived from the nanoindentation measurements for Pr- and Lu-doped ceria. The data for Gd-doped ceria can be found in the literature.[22]

spite of the close size match with Ce^{4+}, is not consistent with the dislocation movement hypothesis. Moreover, there are two regions (3–10% for Lu^{3+} and 10–20% for Pr^{4+}) within which the creep rate is lower than that of ceria and independent of the dopant concentration. These data clearly demonstrate that dislocation movement cannot be the only source of creep at room temperature, if it is present at all.[40–44] These facts agree well with the expectation that, in general, dislocation movement in ceramics should be very slow at room temperature.[45]

We therefore conclude that the initial increase in the creep rate observed for 3 mol% Gd^{3+}- and Pr^{3+}-doped ceria comes from the rearrangement of the O_7–Ce_{Ce}–V_O complexes which

© 2013 WILEY-VCH Verlag GmbH & Co. KGaA, Weinheim

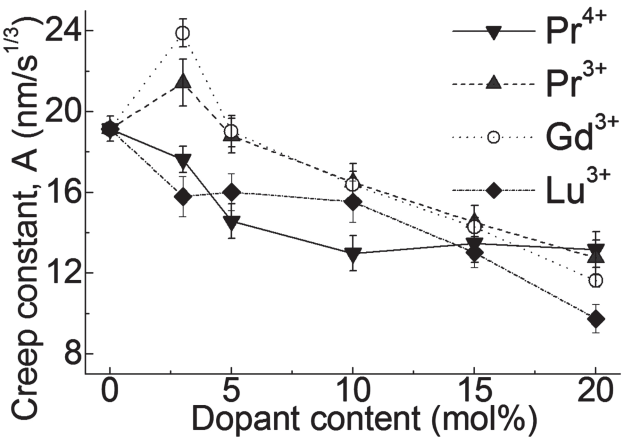

Figure 4. Creep rate constant for Gd-, Lu-, and Pr-doped ceria. The data for Gd-doped ceria can be found elsewhere.[22]

are known to be labile below 200 °C.[7,26,46] This rearrangement has been shown to be the origin of both the chemical strain effect[22,24,30] and the marked electrostrictive behavior[7] of polycrystalline thin films of 20% Gd-doped ceria. With the former, in response to mechanical constraint, strains of 0.2–0.4% as well as dual elastic moduli-relaxed and unrelaxed have been measured, while for the latter, electromechanical activity has been observed at the excitation frequency of 143 Hz.[7] Our more recent, but as yet unpublished, data suggest continuing electromechanical response even at 6 kHz. Therefore, the labile point defect complexes appear to possess the necessary characteristics to explain room temperature creep occurring on a time scale of a few seconds. At dopant concentrations above 3 mol%, the creep is suppressed, likely due to the defect interaction which is accompanied, in the case of the Gd-doped ceria, by the transition to the double fluorite phase (see additional analysis below). The fact that for the ceramics with the two small dopants, Pr^{4+} and Lu^{3+}, the creep rate constant is lower than that of ceria and only weakly dependent on dopant concentration, supports the notion that the appearance of inelastic behavior is due to labile, independent point defect complexes.

According to Rietveld analysis of synchrotron XRD data of Gd^{3+}-doped ceria,[27] oxygen vacancies begin to be correlated for $x \geq 0.1$. Consistent with this finding, we note that at $x = 0.1$, the formation enthalpy of the CeO_2–$GdO_{1.5}$ solid solution and the ionic conductivity both reach a maximum.[35] For $x \geq 0.1$, Artini et al.[27] describe the XRD pattern in terms of the double fluorite unit cell, where there are 16 O2 positions per unit cell. Occupancy of the O2 position (and not the O1 position) decreases linearly with increased doping. The M2–O2 bond lengths do not change, whereas the two M1–O2 bond lengths per unit cell do change. At doping levels below $x = 0.1$, there is no correlation between vacancies, the fluorite structure is maintained on average and vacancies occupy the oxygen positions in a random manner. At 3 mol% doping, 0.75% of the oxygen sites are empty. This is equivalent to 1 vacancy per 128 oxygen positions, which is equivalent to 16 fluorite unit cells or 2.5 unit cells in each of three orthogonal directions. So, on the basis of the XRD results, it would seem that when the vacancy concentration increases by a factor of ≈3 (i.e., vacancies separated by ≈2.5 fluorite unit cells in each of the three orthogonal directions) correlation among the vacancy sites may be initiated. If we argue that correlations among vacancies produce decreased lability of O_7–Me_{Ce}–V_O complexes, and if there is no other contributing factor, then, at $x \geq 0.1$, creep should begin to decrease, as is indeed observed for Gd^{3+}-, Pr^{3+}-, and Lu^{3+}-doped ceria.

3. Conclusions

The results of this study indicate that the size of the dopant, rather than the concentration of vacancies, is a primary determinant of the elastic modulus of doped ceria, even when 5% of oxygen sites are vacant. The creep rate in Gd^{3+}- and Pr^{3+}-doped ceria is largely promoted by the lability of the O_7–Ce_{Ce}–V_O complexes and reaches a maximum at 3 mol% where the defect interaction is minimal. Increase in the concentration of vacancies causes a decrease in the creep rate. Considering the broad, practical applications of ceramic materials with fluorite structure in general, and the importance of doped ceria for miniature fuel cells in particular, we therefore suggest that elastic modulus and creep rate can be controlled by careful selection of dopant radius and concentration. In this regard, nanoindentation is clearly a useful technique for identifying materials with labile point defects,[26] which may point to practical functionality such as high ionic conductivity, large electrostriction, and inelasticity.

4. Experimental Section

$Ce_{1-x}M_xO_{2-x/2}$ (M = Pr^{3+} or Lu^{3+}) powders with x =0, 0.03, 0.05, 0.10, 0.15, and 0.20, were synthesized via a precipitation method, in which a 0.7 M aqueous solution of $(NH_4)_2CO_3$ was added drop-wise to an aqueous solution (0.3 M) containing the required amounts of the corresponding metal nitrate-hexahydrate $M(NO_3)_3{\cdot}6H_2O$ (M = Pr or Lu) (Aldrich, 99.9% purity). The mixture was kept at 80 °C under continuous stirring for 1 h. Then, the precipitates were centrifuged out, triple-rinsed with water and with pure ethanol. The resulting powders were dried at 120 °C for 12 h, ground and annealed in air at 700 °C for 2 h. Cylindrical pellets of 6 mm diameter and 1.2 mm thickness were consolidated from the powders via cold isostatic press at 276 MPa, followed by sintering in air at 1400 °C for 5 h, with heating and cooling rates of 5 °C min^{-1}. The density of all pellets exceeded 95%, as verified by the Archimedes method. The pellets were embedded in metallographic hard resin (EpoKwick, Buehler). Rough polishing was performed with 0.5 μm grain size alumina for more than 5 h (>5 μm removed) followed by fine (50 nm grain size) alumina polish. The resin-embedded pellets were rinsed with industrial detergent in an ultra-sonic bath for 30 min to remove alumina residue. Examination of the samples in a scanning electron microscope (SEM, Leo Supra) indicated that the grain size exceeded 3 μm for all samples. Dopant content in the pellets was confirmed by energy dispersive X-ray fluorescence analysis (EDS). In order to obtain a Pr^{4+}-doped sample, the Pr^{3+}-doped sample was annealed in oxygen for 12 h at 380 °C. The powder XRD patterns were acquired with a Rigaku Ultima III 2theta-theta diffractometer in Bragg-Brentano configuration. All ceramics displayed diffraction patterns consistent with the fluorite phase. The unit cell parameter (a) was calculated using Jade 9 software (MDI, CA) with maximum $2\theta = 120°$.

Nanoindentation measurements were performed at room temperature with an Agilent-XP nanoindenter with a Berkovich (three-sided pyramidal diamond) indenter. To minimize surface effects, all measurements were performed with indentation depth between

© 2013 WILEY-VCH Verlag GmbH & Co. KGaA, Weinheim

800 and 900 nm. The upper limit for the indentation depth was chosen to ensure that it would not exceed approximately half the average grain size. Maximum load of 150 mN was applied using a trapezoidal load–hold–unload cycle (see Figure 2a) at a constant loading/unloading rate: 15 mN s^{-1} ("fast" mode) and 0.15 mN s^{-1} ("slow" mode).[23] At the end of the loading part of the cycle, the load is held constant for a fixed time, 8 s (fast) or 30 s (slow), while the change in displacement due to creep was monitored. Finally, the load was reduced at the same rate as used for loading. The elastic modulus and the nano-hardness were determined using Oliver and Pharr analysis, based on the measured values of the initial slope of the load release curve and the indenter contact area.[20,21] The creep observed during the load hold phase is not expected to influence these values because the rate decreases rapidly enough that, at the end of the load–hold period, the displacement is smaller than the drift. The loading and unloading curves were smooth; there were no "pop-ins",[47] such as are often observed in the presence of cracks or pores at the submicron level, or instabilities (Figure 2b). The requirements for low porosity as well as polishing of high quality were found to be essential for measurement reproducibility.[19,22] Drift rates were measured at 90% unloading in separate experiments and found to be less than 0.1 nm s^{-1}, which is low enough not to significantly influence the results. The influence of any instrumental settling time was also found to be not significant. Each sample was measured twelve times at both loading rates. Elastic modulus, hardness and creep rate were deduced from each curve. Statistically significant measurements (at least eight in each case) were then averaged.

Supporting Information

Supporting Information is available from the Wiley Online Library or from the author.

Acknowledgements

I.L. and S.K. are grateful for financial support from the US-Israel Binational Science Foundation (grant #2008181). I.L. also wishes to thank the Minerva Foundation for funding this research. I.L. gratefully acknowledges the assistance of the Nancy and Stephen Grand Research Center for Sensors and Security, and the Gerhard Schmidt Minerva Center for Supramolecular Architectures at the Weizmann Institute of Science. R.K. expresses his appreciation for the Rahamimoff Travel Grant for Young Scientists. The research is also made possible in part by the generosity of the Harold Perlman Family.

Received: May 6, 2013
Revised: June 3, 2013
Published online: July 2, 2013

[1] M. Mogensen, N. M. Sammes, G. A. Tompsett, *Solid State Ionics* **2000**, *129*, 63.
[2] A. Infortuna, A. S. Harvey, L. J. Gauckler, *Adv. Funct. Mater.* **2008**, *18*, 127.
[3] H. L. Tuller, *Electrochim. Acta* **2003**, *48*, 2879.
[4] M. Greenberg, E. Wachtel, I. Lubomirsky, J. Fleig, J. Maier, *Adv. Funct. Mater.* **2006**, *16*, 48.
[5] A. Kossoy, Y. Feldman, E. Wachtel, I. Lubomirsky, J. Maier, *Adv. Funct. Mater.* **2007**, *17*, 2393.
[6] B. W. Sheldon, V. B. Shenoy, *Phys. Rev. Lett.* **2011**, *106*.
[7] R. Korobko, A. Patlolla, A. Kossoy, E. Wachtel, H. L. Tuller, A. I. Frenkel, I. Lubomirsky, *Adv. Mater.* **2012**, *24*, 5857.
[8] B. Scherrer, J. Martynczuk, H. Galinski, J. G. Grolig, S. Binder, A. Bieberle-Hutter, J. L. M. Rupp, M. Prestat, L. J. Gauckler, *Adv. Funct. Mater.* **2012**, *22*, 3509.
[9] L. J. Gauckler, D. Beckel, B. E. Buergler, E. Jud, U. R. Muecke, M. Prestat, J. L. M. Rupp, J. Richter, *Chimia* **2004**, *58*, 837.
[10] A. Evans, A. Bieberle-Hutter, J. L. M. Rupp, L. J. Gauckler, *J. Power Sources* **2009**, *194*, 119.
[11] J. L. M. Rupp, *Solid State Ionics* **2012**, *207*, 1.
[12] Y. L. Wang, K. Duncan, E. D. Wachsman, F. Ebrahimi, *Solid State Ionics* **2007**, *178*, 53.
[13] H. X. Xu, R. K. Behera, Y. L. Wang, F. Ebrahimi, S. B. Sinnott, E. D. Wachsman, S. R. Phillpot, *Solid State Ionics* **2010**, *181*, 551.
[14] K. Sato, H. Yugami, T. Hashida, *J. Mater. Sci.* **2004**, *39*, 5765.
[15] Y. Wang, K. L. Duncan, E. D. Wachsman, F. Ebrahimi, *J. Am. Ceram. Soc.* **2007**, *90*, 3908.
[16] A. Nakajima, A. Yoshihara, M. Ishigame, *Phys. Rev. B* **1994**, *50*, 13297.
[17] V. Kanchana, G. Vaitheeswaran, A. Svane, A. Delin, *J. Phys.* **2006**, *18*, 9615.
[18] A. Atkinson, A. Selcuk, *Solid State Ionics* **2000**, *134*, 59.
[19] E. Wachtel, I. Lubomirsky, *Scr. Mater.* **2011**, *65*, 112.
[20] W. C. Oliver, G. M. Pharr, *J. Mater. Res.* **1992**, *7*, 1564.
[21] W. C. Oliver, G. M. Pharr, *J. Mater. Res.* **2004**, *19*, 3.
[22] R. Korobko, C. T. Chen, S. Kim, S. R. Cohen, E. Wachtel, N. Yavo, I. Lubomirsky, *Scr. Mater.* **2012**, *66*, 155.
[23] Ref. 22 contains a misprint. The "slow" loading rate was 0.15 mN s^{-1}, that is, ten times slower than the fast rate, similar to the current work.
[24] A. Kossoy, Y. Feldman, R. Korobko, E. Wachtel, I. Lubomirsky, J. Maier, *Adv. Funct. Mater.* **2009**, *19*, 634.
[25] A. Kossoy, A. I. Frenkel, Y. Feldman, E. Wachtel, A. Milner, I. Lubomirsky, *Solid State Ionics* **2010**, *181*, 1473.
[26] A. Kossoy, A. I. Frenkel, Q. Wang, E. Wachtel, I. Lubomirsky, *Adv. Mater.* **2010**, *22*, 1659.
[27] C. Artini, G. Costa, M. Pani, A. Lausi, J. Plaisier, *J. Solid State Chem.* **2012**, *190*, 24.
[28] M. Yashima, S. Kobayashi, *Appl. Phys. Lett.* **2004**, *84*, 526.
[29] M. Yashima, S. Kobayashi, T. Yasui, *Solid State Ionics* **2006**, *177*, 211.
[30] V. Grover, S. N. Achary, A. K. Tyagi, *J. Appl. Crystallogr.* **2003**, *36*, 1082.
[31] A. Banerji, V. Grover, V. Sathe, S. K. Deb, A. K. Tyagi, *Solid State Commun.* **2009**, *149*, 1689.
[32] A. Kossoy, Q. Wang, R. Korobko, V. Grover, Y. Feldman, E. Wachtel, A. K. Tyagi, A. I. Frenkel, I. Lubomirsky, *Phys. Rev. B* **2013**, *87*, 054101.
[33] R. D. Shannon, *Acta Crystallogr. A* **1976**, *32*, 751.
[34] H. Inaba, H. Tagawa, *Solid State Ionics* **1996**, *83*, 1.
[35] H. J. Avila-Paredes, T. Shvareva, W. Q. Chen, A. Navrotsky, S. Kim, *Phys. Chem. Chem. Phys.* **2009**, *11*, 8580.
[36] I. Lubomirsky, *Solid State Ionics* **2006**, *177*, 1639.
[37] D. Marrocchelli, S. R. Bishop, H. L. Tuller, B. Yildiz, *Adv. Funct. Mater.* **2012**, *22*, 1958.
[38] P. Knauth, H. L. Tuller, *J. Eur. Ceram. Soc.* **1999**, *19*, 831.
[39] H. Nitani, T. Nakagawa, M. Yamanouchi, T. Osuki, M. Yuya, T. A. Yamamoto, *Mater. Lett.* **2004**, *58*, 2076.
[40] F. Iguchi, Y. Endo, T. Ishida, T. Yokobori, H. Yugami, T. Otake, T. Kawada, J. Mizusaki, *Solid State Ionics* **2005**, *176*, 641.
[41] J. L. Routbort, K. C. Goretta, A. R. de Arellano-Lopez, J. Wolfenstine, *Scr. Mater.* **1997**, *38*, 315.
[42] S. L. Reis, E. C. C. Souza, E. N. S. Muccillo, *Solid State Ionics* **2011**, *192*, 172.
[43] W. R. Cannon, T. G. Langdon, *J. Mater. Sci.* **1983**, *18*, 1.
[44] W. R. Cannon, T. G. Langdon, *J. Mater. Sci.* **1988**, *23*, 1.
[45] W. D. Kingery, H. K. Bowen, D. R. Uhlmann, *Introduction to ceramics*, Wiley, New York **1976**.
[46] B. Wang, A. N. Cormack, *J. Phys. Chem. C* **2013**, *117*, 146.
[47] M. Morales, J. J. Roa, X. G. Capdevila, M. Segarra, S. Pinol, *Acta Mater.* **2010**, *58*, 2504.

© 2013 WILEY-VCH Verlag GmbH & Co. KGaA, Weinheim